Carbohydrate Polymers 90 (2012) 507–515

Contents lists available at SciVerse ScienceDirect

Carbohydrate Polymers

journal homepage: www.elsevier.com/locate/carbpol

Chondroitin sulfate based nanocomplex for enhancing the stability and activity of anthocyanin

Dooyong Jeong, Kun Na*

Department of Biotechnology, The Catholic University of Korea, 43 Jibong-ro, Wonmi-gu, Bucheon-si, Gyeonggi-do 420-743, Republic of Korea

ARTICLE INFO

Article history:
Received 27 March 2012
Received in revised form 10 May 2012
Accepted 20 May 2012
Available online 28 May 2012

Keywords:
Anthocyanin
Antioxidant
Chondroitin sulfate
Nanocomplex
Intermolecular stacking

ABSTRACT

To improve the structural stability of the potent antioxidant anthocyanin (ATC), a nanocomplex was fabricated from intermolecular stacking between chondroitin sulfate (CS) and ATC using a simple complexing method in water, without inputting high energy or an organic solvent. The physicochemical properties of the nanocomplex were evaluated at various feed weight ratios of CS/ATC. The most stable nanocomplex was obtained at a CS/ATC weight ratio of 10/1 (WR10). The ATC loading content and loading efficiency were 6.3 and 99%, respectively. Its diameter was approximately 300 nm with unimodal size distribution. The intermolecular stacking state of WR10 was maintained up to 1 μg/ml of ATC, whereas an intermolecular stacking state formed by ATC alone was easily dissociated below 16 μg/ml of ATC. The structural stability of ATC in WR10 was 8 times higher than that of free ATC at 37 °C. Moreover, the complex effectively protected the ATC degradation by hydroxyl molecules under high pH (above 9) conditions. Finally, cancer cell growth suppression activity was measured to determine the in vitro free radical scavenger ability of ATC. The WR10 strongly suppressed the Hela cell growth compared with ATC alone. Therefore, we conclude that the CS/ATC nanocomplex has a potential for use as a carrier for stable antioxidants or water-soluble drugs via intermolecular stacking. These nanocomplexes would prove useful for applications in the food and pharmaceutical industries.

1. Introduction

Recently, oxidative stress, which is caused by reactive oxygen species (ROS), has gained increasing attention due to its associations with many chronic diseases (Gangestad, Merriman, & Emery Thompson, 2010). Oxidative stress is related to cancer (Klaunig et al., 1998), diabetes (Newsholme et al., 2007), Alzheimer's disease (Smith, Rottkamp, Nunomura, Raina, & Perry, 2000), Parkinson's disease (Jenner, 2003), amyotrophic lateral sclerosis (ALS) (Ferrante et al., 1997) and other human diseases. Therefore, a decrease in ROS levels in body fluids is an important goal for current medicines and therapies.

Many antioxidants have been studied for their potential to reduce oxidative stress (Kähkönen et al., 1999; Rice-Evans, Miller, & Paganga, 1996). Antioxidant enzymes (Jaruga, Zastawny, Skokowski, Dizdaroglu, & Olinski, 1994) and low molecular weight natural compounds (Rice-Evans, Miller, & Paganga, 1997) have primarily been used to remove ROS. However, regardless of high antioxidant efficacy, the use of enzymes is limited to industrial applications because of their high cost and the difficulty in obtaining large quantities (Montenecourt & Eveleigh, 1979).

Alternatively, anthocyanin (ATC), a low molecular weight natural compound, has high free radical scavenging capacity with a low redox potential (0.23–0.75) (Pietta, 2000). ATC has various pharmacological properties, such as anti-aging (Bagchi, Sen, Bagchi, & Atalay, 2004), anti-inflammatory (Kong, Chia, Goh, Chia, & Brouillard, 2003), antibacterial (Kowalczyk, Krzesiński, Kura, Szmigiel, & Blaszczyk, 2003), anti-tumorigenic (Wang & Stoner, 2008), and anti-carcinogenic (Bagchi et al., 2004) effects. Moreover, it is easily extracted from many plants and vegetables, such as grapes or black beans (Ichikawa et al., 2001). On the basis of these advantages, ATC has been suggested for use in pharmacological compounds.

Despite the many pharmacological effects of ATC, it has a chemically unstable structure that is influenced by pH, temperature, light (Laleh, Frydoonfar, Heidary, Jameei, & Zare, 2006) and concentration. Therefore, ATC has a very short half-life and low bioavailability (Frank et al., 2007).

A co-pigmentation reaction has been used to improve the stability of ATC (Brouillard, Wigand, Dangles, & Cheminat, 1991; Mistry, Cai, Lilley, & Haslam, 1991) using low molecular weight natural compounds such as gallic acid or caffeic acid as co-pigments (Eiro & Heinonen, 2002). Gris, Ferreira, Falcão, and Bordignon-Luiz

* Corresponding author at: Nano Biomedical Polymer Research Laboratory, Department of Biotechnology, The Catholic University of Korea, 43-1 Yeokgok 2-dong, Wonmi-gu, Bucheon-si, Gyeonggi-do 420-743, Republic of Korea.
Tel.: +82 2 2164 4832; fax: +82 2 2164 4865.
E-mail address: kna6997@catholic.ac.kr (K. Na).

0144-8617/$ – see front matter © 2012 Elsevier Ltd. All rights reserved.
http://dx.doi.org/10.1016/j.carbpol.2012.05.072

(2007) reported on the stabilization of ATC using caffeic acid as a co-pigment under various storage conditions. The stabilization mechanism of the co-pigmentation reaction involves maintenance of the intermolecular stacking state of ATC that results from charge interactions with the co-pigment (Figueiredo & Pina, 1994) and the formation of a hydrophobic core (Davies & Mazza, 1993) that is caused by π–π stacking (Berke & de Freitas, 2005). This mechanism prevents the hydration of ATC and maintains the quinoidal-base (qb) or flavylium cation structure, rather than a carbinol or chalcone structure (Gris et al., 2007). Although the co-pigment forms a complex with ATC, it is easily dissociated at elevated temperature or by the action of a solvent (Boulton, 2001). Another approach for the stabilization of ATC is the introduction of a nanocarrier system. Liposomes, cyclodextrin, polymeric nanoparticles and simple emulsions could be used as nanocarriers of encapsulated ATC (Fang & Bhandari, 2010). These carriers can serve many functions, such as sustained release (Shi & Li, 2005), targeted delivery (Mohanraj & Chen, 2007) and extended half-life (Zhang et al., 2007) in vivo. However, nanocarriers face different challenges from those of the co-pigmentation reaction in the manufacturing process, especially if the use of organic solvents or high energy is required to synthesize nanocarriers. When considering the main factor that contributes to the degradation of ATC, organic solvents and high energy are unsuitable for the stabilization of ATC.

Here, we propose a novel nanocomplex using sulfated polysaccharide for the stabilization of ATC. Sulfated polysaccharide has a strong negative charge on its surface that could maintain charge interaction with ATC and a stacking structure even at extremely low concentrations.

We considered chondroitin sulfate (CS), a member of the glycosaminoglycan (GAG) family and an acidic mucopolysaccharide found in cartilage, skin, corneas, and umbilical cords (Lee et al., 2007), as a potential candidate for long-term ATC stabilization. CS is capable of forming ionic complexes with positively charged ATC. Moreover, CS has many promising properties such as biocompatibility, biodegradability, anti-inflammatory effects, and a High level of structure/disease-modifying anti-osteoarthritis activity (Huang et al., 2009). CS has many sulfate and *N*-acetyl residues. The sulfate groups of CS generate hydrophilic surfaces on the nanocomplex and provide good colloidal stability. In addition, the *N*-acetyl groups of CS may help the intermolecular stacking of ATC because of its hydrophobicity. Additionally, we assumed that CS may improve the stability of ATC because of its high molecular weight. Contrary to lower molecular weight co-pigments, CS acts as a stabilizing agent to maintain the stacking configuration of ATC because of its high charge density.

In this study, a nanocomplex induced by an intermolecular stacking interaction between CS and ATC was designed, and its physicochemical properties, such as particle size, zeta potential, and ATC loading efficiency, were measured at various weight ratios of CS/ATC and at various pHs. Additionally, the free radical scavenging activity of the complex was evaluated by the removal rate of 2,2-diphenyl-1-picrylhydrazyl (DPPH) and by determining the effects of CS/ATC nanocomplex on free radical-induced of cancer cell growth.

2. Materials and methods

2.1. Materials

Chondroitin sulfate was purchased from Carl Roth (Schoemperlenstra, Karlsruhe, Germany). Black soybean ATC was provided by the rural development administration of Korea. The compounds 2,2-diphenyl-1-picrylhydrazyl (DPPH), dichlorofluorescein diacetate (DCF-DA), lipopolysaccharide (LPS) and all other chemicals were purchased from Sigma Aldrich (St. Louis, MO, USA).

2.2. Formation of CS–ATC nanocomplexes

ATC was dissolved in a water/ethanol solution (1:1, v/v), and the ethanol was evaporated at 60 °C for 30 min. For this process, the stability of ATC maintained approximately 97 wt% (Fig. S1). To remove the remaining insoluble impurities in the solution, ATC in the water was filtered using a 0.45 μm syringe filter. The CS/ATC nanocomplex was formed by adding the ATC solution into the CS solution at a desired complex ratio. All experiments in this study were performed 3 h after the complex formation.

2.3. Confirmation of CS–anthocyanin nanocomplex formation

The formation of nanocomplexes was confirmed by our previously described method with simple modifications (Kim & Na, 2010). The CS/ATC were characterized by the weight ratio (WR) of CS to ATC (i.e., WR0.1 equals a CS–ATC weight ratio of 0.1:1), ranging from WR0.1-10. The complexes remained at room temperature for 3 h, and the turbidity was measured using a UV/vis spectrophotometer (UV-2450, Shimadzu Corporation, Kyoto, Japan) at 600 nm. The lowerst nanocomplex forming CS/ATC WR was also evaluated using a fluorospectrometer (EX: 513 nm, EM: 514 nm). The ATC content and the loading efficiency of the CS/ATC nanocomplex were determined by the absorbance of unloaded ATC. The unloaded compound was extracted by centrifugation in an amicon tube (MwCO: 3500, Millipore®) at 3000 rpm for 10 min. The absorbance of the unloaded compound was detected at 523 nm. Finally, the ATC content and loading efficiency were calculated by following equations:

$$\text{ATC content (\%)} = \frac{\text{weight of loaded ATC}}{\text{total weight of CS/ATC nanocomplex}} \times 100, \quad \text{(A.1)}$$

$$\text{ATC loading efficiency (\%)} = \frac{\text{feed ATC} - \text{unloaded ATC)}}{\text{feed ATC}} \times 100. \quad \text{(A.2)}$$

2.4. CS/ATC nanocomplex size measurement

Dynamic light scattering (DLS) (Malvern, Nanosizer) was used to measure the hydrodynamic diameter and size distribution of the CS/ATC nanocomplex. The intensity autocorrelation was measured at a scattering angle (θ) of 90° at 25 °C. The ATC concentration in the sample was maintained at 0.1 mg/ml. All samples were measured in triplicate and averaged.

2.5. Intermolecular stacking of ATC

Intermolecular stacking of ATC was confirmed by the absorbance spectrum of the CS/ATC nanocomplex. Each complex that contained equal amounts of ATC was considered to be a sample. The absorbance spectra for all samples were obtained at 350–750 nm.

2.6. Minimum intermolecular stacking concentration

The nanocomplexes constructed from CS/ATC ratios of 10/1, 8/1, 6/1 of CS/ATC were used for determining the minimum intermolecular stacking concentrations. A working solution of ATC at 0.5 mg/ml contained each complex solution and was diluted to final ATC concentrations ranging between 0.002 mg/ml and 0.5 mg/ml. Absorbance measurements were performed at room temperature using a UV/vis spectrophotometer. The absorbance

of each sample was recorded at 522 nm for the nanocomplex and 513 nm for free ATC. Additionally, differences in the minimum intermolecular stacking concentration of free ATC and CS/ATC nanocomplex were confirmed by scanning electron microscopy (SEM).

2.7. Stabilization of ATC in PBS solution at 37 °C

The stabilization of ATC was confirmed in 0.01 M phosphate buffered saline (PBS, pH7.4) at 37 °C. A volume of 3 ml of CS/ATC nanocomplex solution or free ATC solution was mixed with an equal volume of 0.02 M PBS solution (pH 7.4). The mixture was placed in a 37 °C shaking water bath. The samples were removed at the appropriate time intervals for quantification of the quinoidal-base or flavylium cation structured ATC. The samples were freeze-dried, re-dissolved in methanol and filtered to obtain pure ATC in solution. The remaining ATC content was determined by UV/vis spectrophotometer at 523 nm.

2.8. Stabilization of ATC in solution at various pHs

ATC stabilization was evaluated at various pHs at room temperature. A volume of 3 ml of CS/ATC nanocomplex solution or free ATC solution was mixed with an equal volume of buffer solutions of varying pH. The ionic strength of the buffer solution was fixed at 0.15 M. The mixture was maintained at room temperature for 1 h and then freeze-dried and re-dissolved in methanol to obtain pure ATC in solution. The remaining ATC content was determined by reverse phase-HPLC-UV. HPLC analysis was performed using a C18 column (15 cm × 0.46 cm, 300 Å, 5 μm particle size, Abbota, USA) with a variable wavelength detector at 523 nm.

2.9. Free radical scavenging activity of the CS/ATC nanocomplex

The free radical scavenging activity of the CS/ATC nanocomplexes and free ATC was tested spectrophotometrically with ELISA by measuring the disappearance of the DPPH radicals at 517 nm. A volume of 50 μl of complex solution, containing 0.025 mg of ATC, was prepared in a 96-well plate. Equal amounts of ATC were used as a control against the CS/ATC nanocomplex. Ten minutes after the addition of 100 μl of 0.5 μM DPPH radicals, the absorbance was measured at 517 nm. The DPPH radical scavenging efficiency was calculated using the following equation:

$$\text{DPPH radical scavenge efficiency (\%)} = \frac{A_0 - A_1}{A_0} \times 100, \qquad \text{(B.1)}$$

where A_0 is the initial absorbance of the added DPPH radicals, and A_1 is absorbance of the remaining DPPH radicals in the presence of the CS/ATC nanocomplex or free ATC.

2.10. Suppression of cancer cell proliferation

Hela cells were used as a model cancer cell line to evaluate the antioxidant effects of the CS/ATC nanocomplex or free ATC under in vitro conditions. A cell count of 1×10^4 of Hela cells was cultured in a 96-well plate in RPMI 1640 media containing 10% fetal bovine serum and 1% antibiotics. One day after seeding the Hela cells on the 96-well plate, 6.25 μg of LPS was mixed with 50 μl of solution containing the nanocomplexes or free ATC and added to each well. The media were extracted 24 h later to use for quantification of ROS, and the cells in the plate were assayed for cell viability against LPS-induced ROS.

DCF-DA was used as a fluorescent probe for quantification of ROS in the cell media. Briefly, 50 μl of 0.2 mM DCF-DA were added to 100 μl of media. Ten minutes after the addition of DCF-DA, the fluorescence intensity was measured at an excitation wavelength of 488 nm and an emission of 510 nm using a fluorescent plate reader.

Cell viability was determined using an MTT assay. A volume of 80 μl of fresh RPMI 1640 media was added into the upper 96-well plates, and then 20 μl of MTT solution was added. After 2 h of incubation, all media were removed and, 100 μl of DMSO was added to the plate. The absorbance of the generated formazan was detected at 495 nm using ELISA.

2.11. Statistical analysis

Statistical analysis of the experimental data was performed using Student's *t*-test, and the results are presented as the

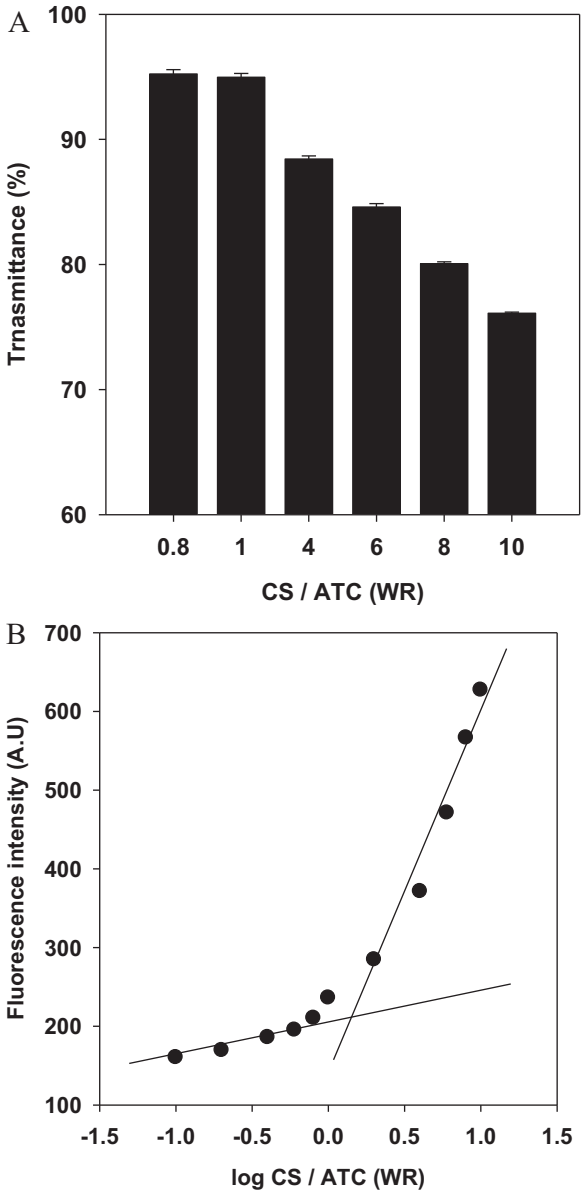

Fig. 1. CS–ATC nanocomplex formation: (A) transmittance of CS/ATC nanocomplexes against various CS–ATC complex ratios. (B) Fluorescence intensities of CS/ATC nanocomplexes.

mean ± SD. Statistical significance was accepted at a level of $p < 0.005$.

3. Results

3.1. Formation of CS/ATC nanocomplexes

Three hours after the addition of CS, increased turbidity in the CS/ATC solution was observed. The transmittance of CS/ATC complexes was significantly decreased from WR4 to WR10 but not from WR0.8 to WR1 (Fig. 1A). The ratio of CS/ATC that successfully results in the formation of nanocomplexes was determined by the fluorescence intensity of ATC (Fig. 1B). ATC has two differential tendencies with WR2 complexes as the center. The straight line above WR2 has a higher gradient than that below WR2. The complex size was measured by dynamic light scattering (DLS). WR10 has a monodisperse size distribution (Fig. 2A). The hydrodynamic volume of the complex increased at WRs above WR4. Finally, WR6, WR8 and WR10 complexes exhibited size distributions ranging from 200 nm to 300 nm (Fig. 2B). The PDI value of the complex size was significantly less than 0.4 for the WR6, WR8 and WR10 complexes.

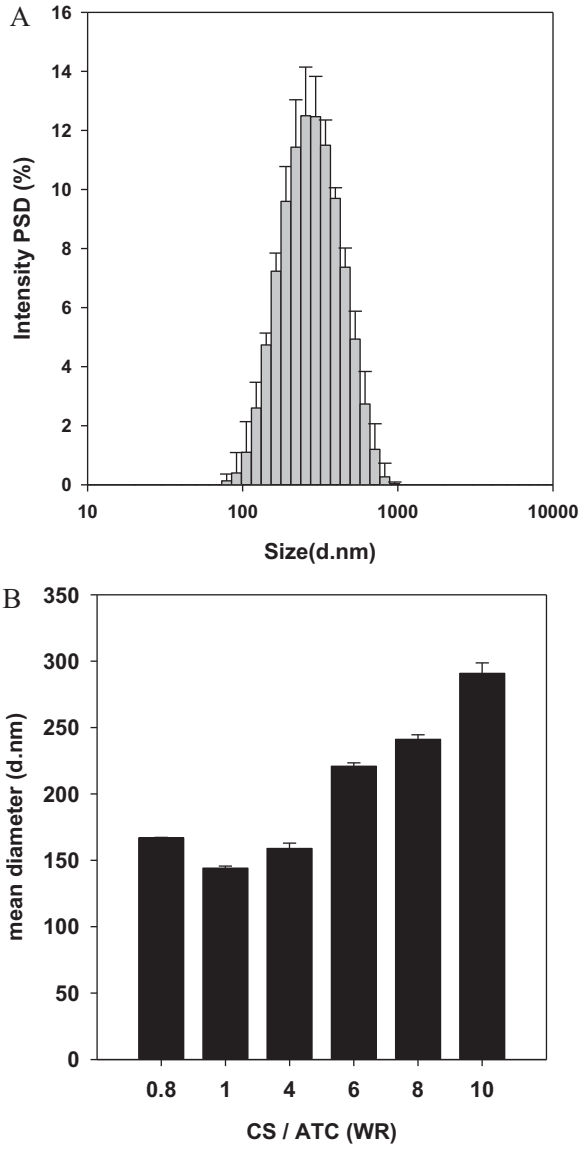

Fig. 2. Characterization of CS/ATC nanocomplexes: (A) size distribution of CS/ATC nanocomplexes (WR10). (B) Hydrodynamic diameter of CS/ATC nanocomplexes. All samples contained 0.1 mg/ml of ATC.

3.2. Observation of intermolecular stacking interactions

Absorbance spectra were used to confirm the stacking state of each CS/ATC nanocomplex (Fig. 3A). In the spectra, the absorbance of ATC decreased from WR0.8 to WR1 and increased from WR4 to WR10. Additionally, a bathochromic shift was observed in the absorbance spectra from 513 nm to 522 nm in WR4–WR10, but not in WR0.8–WR1. When the CS solution was added to the ATC solution, the color of the ATC rapidly changed from red to purple (Fig. 3B). The minimum intermolecular stacking concentration was defined by the absorbance intensity (Fig. 4A). As with WR10, the WR8 and WR6 complexes exhibit one stacking configuration, even though they contained extremely low concentrations of ATC. Conversely, the free ATC demonstrated two configurations with 16 μg/ml of ATC as the center. Above this concentration, the stacking was structured, and below this concentration, the intermolecular stacking of free ATC was dissociated. In the SEM investigation, CS/ATC nanocomplex and free ATC particles were evaluated at 500 μg/ml (Fig. 4B and D). The CS/ATC nanocomplex maintained its morphology below 5 μg/ml (Fig. 4C), but the free ATC did not (Fig. 4E). In the SEM image of 5 μg/ml of free ATC, intermolecular stacking was gradually dissociated, and the size of the nanocomplex became smaller.

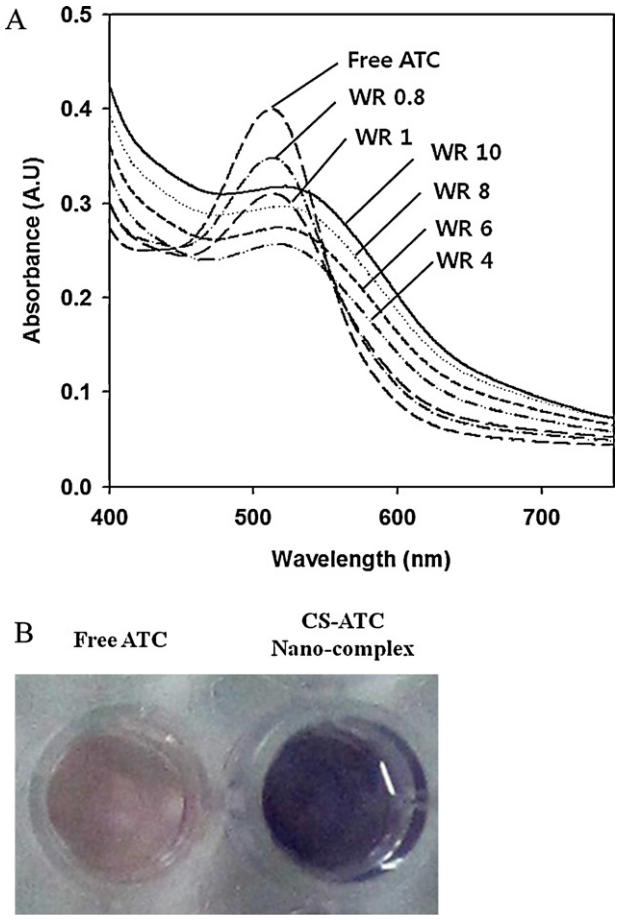

Fig. 3. Optical characteristics of CS/ATC nanocomplexes: (A) absorbance spectrum of CS/ATC nanocomplexes. (B) Photograph of free ATC (red) and WR10 CS/ATC (blue) loaded nanocomplex taken with a digital camera. Bluing effect (bathocromic shift) of ATC was shown in CS-ATC nanocomplex.

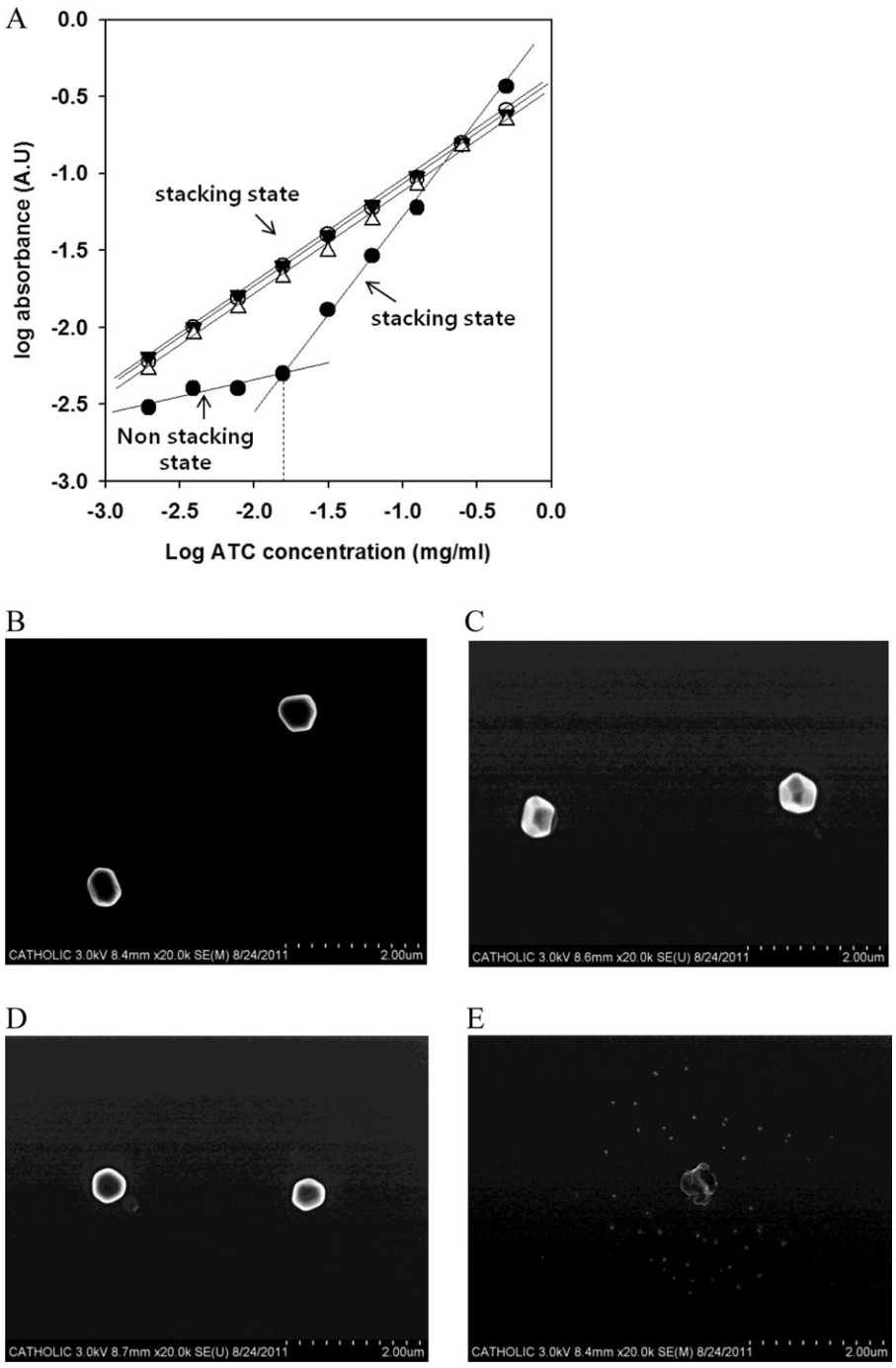

Fig. 4. Intermolecular stacking concentration of ATC: (A) minimum intermolecular stacking concentration of ATC. Free ATC, (●); WR10 CS/ATC nanocomplex, (○); WR8 CS/ATC nanocomplex, (▼); WR6 CS/ATC nanocomplex, (△) (B) SEM image of 500 μg/ml of ATC-containing WR10 CS/ATC nanocomplex. (C) SEM image of 5 μg/ml of ATC-containing WR10 CS/ATC nanocomplex (D) SEM image of 0.5 mg/ml of free ATC (E) SEM image of 0.005 mg/ml of free ATC. The scale bar indicates 2 μm.

3.3. Stability of ATC at 37 °C in PBS under various pH conditions

To confirm the stability of ATC, non-degraded quinoidal-base or flavylium cation-structured ATC was quantified by UV/vis spectrophotometry at 523 nm. In the PBS solution (pH 7.4, 37 °C) ATC was stabilized via CS/ATC complex formation. Free ATC was degraded by 37% within 6 h. Conversely, CS in the CS/ATC complex (WR10) prevented the degradation of ATC. After 2 days, ATC in the CS/ATC complex was degraded by only 18%, while the free ATC had degraded by 85% (Fig. 5A). In general, increasing the pH led to increased ATC degradation. Approximately 87% of free ATC remained in the solution at pH 6, while only 33% remained in solution at pH 12. The nanocomplex protected the ATC from pH-related degradation. The solution containing the CS/ATC nanocomplex (WR10) maintained 78% of its ATC content at pH 12 (Fig. 5B). The colors of the quinoidal base (qb) (red) and flavylium cation-(blue) structured anthocyanin were observed in the CS/ATC nanocomplexes but not in free ATC at pH 9 and pH 12 (Fig. 5C).

3.4. Free radical scavenging activity of CS/ATC nanocomplexes

In the DPPH radical scavenging assay, WR10, WR8 and WR6 exhibited 73.4%, 72.8% and 69.9% radical scavenging efficiency,

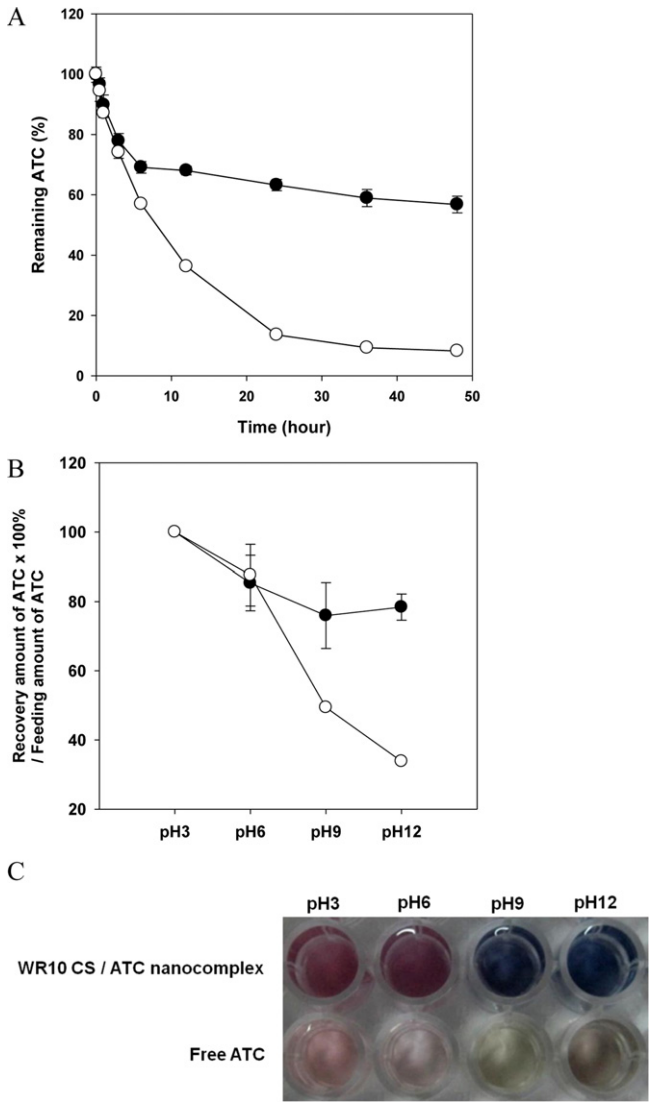

Fig. 5. ATC stability in PBS at 37 °C or various pHs. (A) Quantification of quinoidal base- or flavylium cation-structured ATC in PBS (pH 7.4) at 37 °C. (B) Quantification of quinoidal base- or flavylium cation-structured ATC in buffers of varying pHs. Free ATC, (○); WR10 CS/ATC nanocomplex, (●). (C) Photographic image of WR10 CS/ATC complex and free ATC in buffers of varying pHs. The stable flavylium cation (red, pH3-6) and quinoidal base structred ATC (blue, pH9-12) were observed in the case of WR10 CS/ATC nanocomplex, while the free ATC was finally degraded (brown, pH12) via carbinol base (colorless, pH6) and chalcone structured ATC (yellow pH9).

respectively. The free ATC only demonstrated an efficiency of 35.7% (Fig. S2).

3.5. Suppression of cancer cell proliferation

Lipopolysaccharide (LPS) mediated ROS was quantified by the DCF-DA assay (Fig. 6A). ROS was significantly increased by LPS treatment. In the LPS only-treated media, 202% of ROS was detected. ATC played an important role in reducing the oxidative stress. In free ATC-treated media, the ATC reduced ROS concentrations to 140%. The CS/ATC nanocomplex had an even stronger effect on reducing the oxidative stress. WR10-treated media exhibited an ROS intensity of 115%. It is well known that ROS facilitates cancer cell growth. Thus, the cell growth suppression by ATC was also evaluated to determine the biological activity of ATC (Burdon & Gill, 1993). LPS only treated Hela cells were grown to 186% (Fig. 6B). Free ATC reduced cancer cell proliferations to 147%, but the CS/ATC

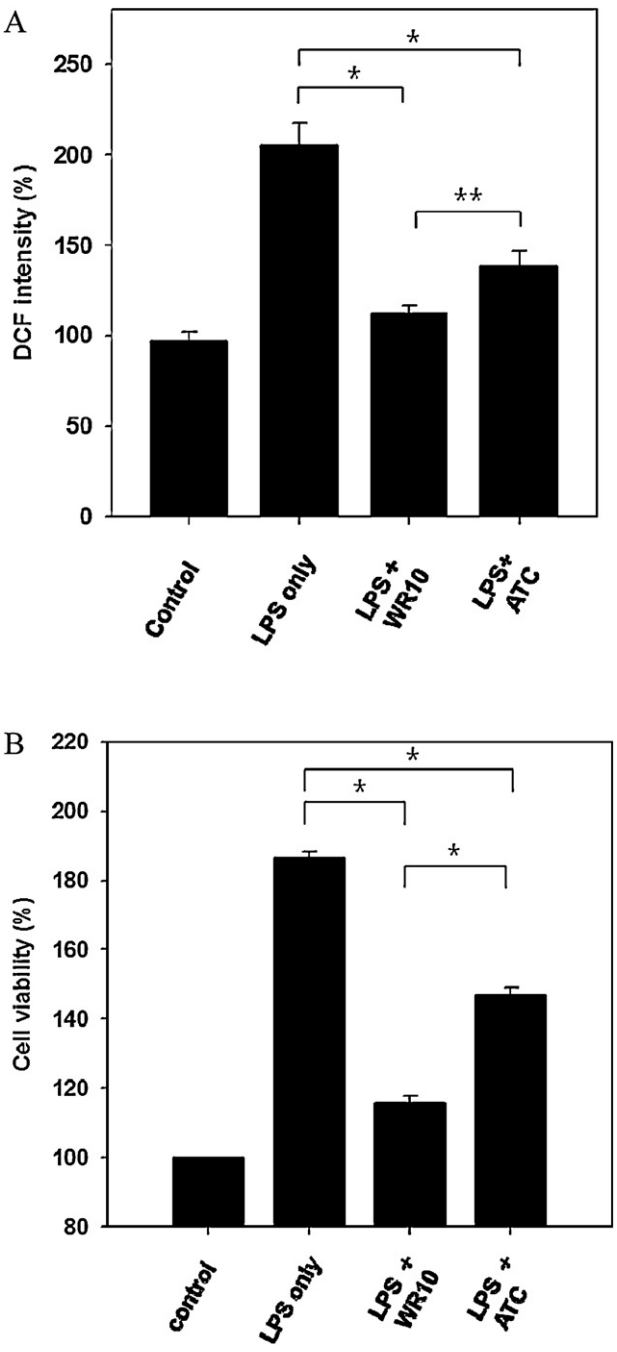

Fig. 6. In vitro antiproliferative activities of CS/ATC nanocomplex. (A) Radical scavenging rate in HeLa cell culture media. (B) HeLa cell viability was determined with an MTT assay ($^{*}p < 0.0001$, $^{**}p < 0.005$, $n = 3$).

nanocomplex demonstrated a much stronger effect on cell growth inhibition.

4. Discussion

In this study, we proposed a new concept for ATC stabilization. CS was used to establish a charge complex with ATC. The CS/ATC nanocomplex was prepared by a very simple, rapid process. Unlike general polymeric nanoparticles or vehicles, the nanocomplex was formed by intermolecular stacking forces and charge interactions. Generally, polymeric nanoparticles have hydrophobic residues on the polymer, but CS exhibited good solubility in water due to the numerous sulfate groups on its glucose backbone.

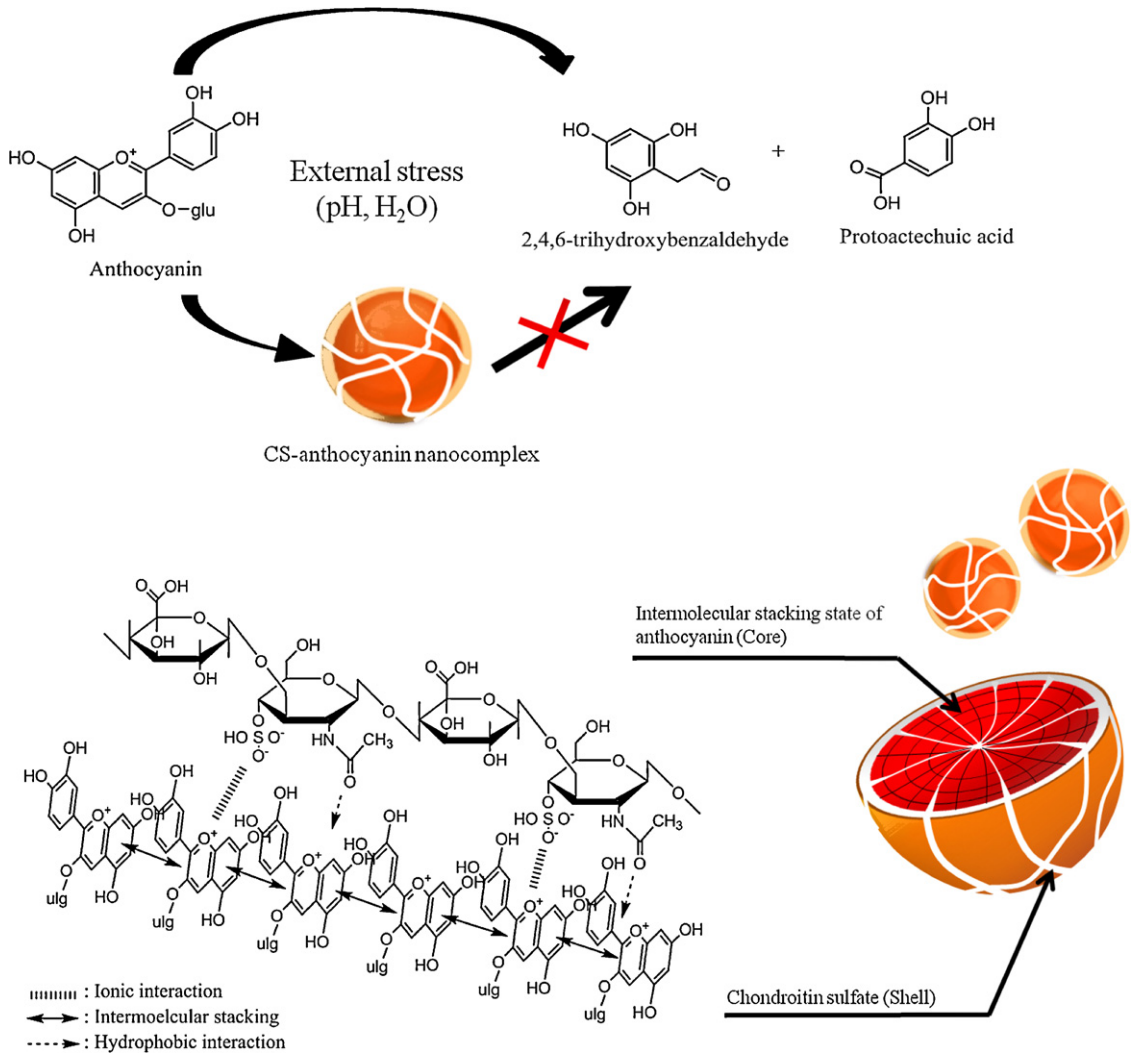

Fig. 7. Schematic illustration of the CS/ATC nanocomplex.

Therefore, it did not require any additional energy to establish the nanocomplex. Furthermore, because the intermolecular stacking of ATC was formed by π–π interactions in the water, the CS/ATC nanocomplex formation process does not require the use of organic solvents. When considering factors that degrade ATC, such as heat, light, high pH, and organic solvents, this nanocomplex-forming process is a suitable method for ATC loading.

The complex formation was determined by transmittance and fluorescence intensities of ATC. Transmittance was decreased because the nanosized complex was formed. Fluorescence intensities were significantly increased when the WR was above 2, due to intermolecular stacking interaction of ATC in the nanocomplexes. At WR above 10, the nanocomplexes became aggregated and precipitated (data not shown). Taken together, most stable CS/ATC intermolecular stacking nanocomplexes with dimensions of 200–300 nm in water were formed at WR10. Thus, WR10 was used for subsequent experiments.

We assumed that three interactions including (i) intermolecular stacking interactions, (ii) hydrophobic interactions and (iii) ionic interactions existed in the nanocomplexes (Fig. 7). The π–π stacking force plays a critical role in ATC stabilization (Berke & de Freitas, 2005). In other studies, intermolecular stacking interactions prevented the degradation of ATC. ATC was hydrated twice from the quinoidal-base (qb) or the flavylium cation structure to finally generate 2,4,6-trihydroxybenzaldehyde and protocatechuic acid (Seeram, Bourquin, & Nair, 2001). Intermolecular stacking interactions prevent hydration of ATC via the formation of a hydrophobic core (Davies & Mazza, 1993). Eiro and Heinonen (2002) and Goto, Tamura, Kawai, Hoshino, Harada, and Kondo (1986) studied the bathochromic and hyperchromic shift of ATC in co-pigmentation reactions. These absorbance shifts were well known as typical phenomena associated with intermolecular stacking and ATC stabilization. However, in our study, hypochromic shift was observed for WR4 and below, whereas bathochromic and hyperchromic shift of ATC was observed for WR4–WR10 (Fig. 3A). From these results, we assumed that CS contributes to disintegration (below WR4) and rearrangement (above WR4) of intermolecular-stacked ATC via charge–charge interactions. The color changes between free ATC and CS/ATC nanocomplexes induced the absorbance shift (Fig. 3B). Moreover, ATC loading was successfully achieved in the WR10 CS/ATC nanocomplex without significant losses of ATC (Table 1). This result means that the system may be useful for hydrophilic drug delivery.

The second interaction of the CS/ATC nanocomplex is the hydrophobic interaction between the acetyl groups on CS and the stacked anthocyanin. In general, hydrophobic interactions influence the stabilization of the nanocomplex. ATC is a self-stacking molecule at high concentrations; thus, the stability of ATC was influenced by its concentration. In these data, free ATC has two tendencies, with 16 μg/ml of ATC at the center. Above 16 μg/ml of

Table 1
ATC loading efficiency and contents in CS/ATC nanocomplexes.

Sample name	Feed ATC amount (±SD[a])	Drug contents (±SD)	Loading efficiency (±SD)	Unloaded ATC (±SD)
10:1 CS/ATC complex	0.678 mg (±0.010)	6.279% (±0.087)	98.820% (±0.290)	0.008 mg (±0.002)

[a] Standard deviation ($n = 3$).

ATC, a well-maintained stacked state is observed, whereas a dissociated state is observed below this concentration. However, the CS/ATC nanocomplex was stabilized by the intermolecular stacking of ATC at the extremely low concentrations. Likewise, SEM data show these strong intermolecular stacking interactions of CS/ATC nanocomplexes, as demonstrated in the difference in morphology between CS/ATC nanocomplexes and free ATC particles at low concentrations (Fig. 4C and E).

Finally, charge-charge interactions between sulfate and carboxylic groups in CS and quinoidal-base (qb) or flavylium cation structured ATC contributed to strong nanocomplexation. The CS caused the intermolecular ATC stacking to be tightly woven and provided a strong interaction between each of the stacked ATC molecules.

ATC was stabilized by the CS/ATC nanocomplex at 37 °C in PBS or various pHs. Therefore, stable ATC structures, such as quinoidal-base (qb) and flavylium cation structures were detected in the CS/ATC complex. The stabilization effects were also supported by the color changes of the CS–ATC nanocomplex or free ATC at various pHs (Fig. 5C). The CS/ATC nanocomplex has two colors, which represent flavylium cation (red) and quinoidal base (blue) structure, whereas the free ATC has four colors. In the case of free ATC, the compound was finally degraded (brown) via a carbinol base (colorless) and chalcone structure (yellow). To summarize these results, we assumed that the hydration or degradation of ATC was prevented by both intermolecular stacking and hydrophobic interactions within the CS/ATC nanocomplex, whereas free ATC was easily changed by various experimental conditions.

To measure the free radical scavenging activity of ATC, DPPH radicals were measured. The DPPH radical scavenging assay has been widely used to compare the free radical scavenging activity of natural compounds in many previous studies (Brand-Williams, Cuvelier, & Berset, 1995). In our results (Fig. S2), the CS/ATC complex demonstrated higher free radical scavenging activity than free ATC. The strong radical scavenging effect may be a result of ATC protection in the water. When the free ATC was exposed to water, degradation commenced immediately as a result of its hydration. The CS/ATC nanocomplex was formed very quickly such that the ATC was protected from hydration.

The free radical scavenging activity in vitro was confirmed using HeLa cells. Intra- or extracellular ROS act as signaling molecules in HeLa cell proliferation (Burdon & Gill, 1993). On the basis of this study, LPS-mediated ROS generation was detected using the fluorescence probe DCF-DA. The CS/ATC complex provided greater protection than free ATC in reducing the LPS-induced ROS (Fig. 6A). Thus, HeLa cell proliferation was effectively inhibited by the strong antioxidant activities of the CS/ATC complex (Fig. 6B).

5. Conclusion

A CS/ATC nanocomplex was prepared by a simple process without the use of additional energy or organic solvents. The CS/ATC nanocomplex protects the ATC structure from degradation at 37 °C and in PBS under various pH conditions because of intermolecular stacking interactions, hydrophobic interactions and charge–charge interactions. CS tightly weaved ATC together so that the nanocomplex maintained its structure without the dissociation of ATC, even at extremely low ATC concentrations. Moreover, the CS/ATC nanocomplex effectively inhibited the proliferation of cancer cells (HeLa) compared with free ATC. Therefore, the CS/ATC nanocomplex has promising potential for use in pharmaceutical compounds.

Acknowledgements

This research was financially supported by the Next-Generation BioGreen 21 program (PJ007186201002) and the Korean Ministry of Education, Science and Technology through Strategic Research (2011-0028726) and by research funds from The Catholic University of Korea (Research Fund 2012).

Appendix A. Supplementary data

Supplementary data associated with this article can be found, in the online version, at http://dx.doi.org/10.1016/j.carbpol.2012.05.072.

References

Bagchi, D., Sen, C., Bagchi, M., & Atalay, M. (2004). Anti-angiogenic, antioxidant, and anti-carcinogenic properties of a novel anthocyanin-rich berry extract formula. *Biochemistry (Moscow)*, *69*(1), 75–80.

Berke, B., & de Freitas, V. A. P. (2005). Influence of procyanidin structures on their ability to complex with oenin. *Food Chemistry*, *90*(3), 453–460.

Boulton, R. (2001). The copigmentation of anthocyanins and its role in the color of red wine: A critical review. *American Journal of Enology and Viticulture*, *52*(2), 67–87.

Brand-Williams, W., Cuvelier, M., & Berset, C. (1995). Use of a free radical method to evaluate antioxidant activity. *LWT-Food Science and Technology*, *28*(1), 25–30.

Brouillard, R., Wigand, M. C., Dangles, O., & Cheminat, A. (1991). pH and solvent effects on the copigmentation reaction of malvin with polyphenols, purine and pyrimidine derivatives. *Journal of the Chemical Society, Perkin Transactions 2*, (8), 1235–1241.

Burdon, R. H., & Gill, V. (1993). Cellularly generated active oxygen species and HeLa cell proliferation. *Free Radical Research*, *19*(3), 203–213.

Davies, A., & Mazza, G. (1993). Copigmentation of simple and acylated anthocyanins with colorless phenolic compounds. *Journal of Agricultural and Food Chemistry*, *41*(5), 716–720.

Eiro, M. J., & Heinonen, M. (2002). Anthocyanin color behavior and stability during storage: Effect of intermolecular copigmentation. *Journal of Agricultural and Food Chemistry*, *50*(25), 7461–7466.

Fang, Z., & Bhandari, B. (2010). Encapsulation of polyphenols – A review. *Trends in Food Science & Technology*, *21*(10), 510–523.

Ferrante, R. J., Browne, S. E., Shinobu, L. A., Bowling, A. C., Baik, M. J., MacGarvey, U., et al. (1997). Evidence of increased oxidative damage in both sporadic and familial amyotrophic lateral sclerosis. *Journal of Neurochemistry*, *69*(5), 2064–2074.

Figueiredo, P., & Pina, F. (1994). Formation of anthocyanin ion-pairs. A copigmentation effect. *Journal of the Chemical Society, Perkin Transactions 2*, (4), 775–778.

Frank, T., Janssen, M., Netzel, G., Christian, B., Bitsch, I., & Netzel, M. (2007). Absorption and excretion of elderberry (*Sambucus nigra* L.) anthocyanins in healthy humans. *Methods and Findings in Experimental and Clinical Pharmacology*, *29*(8), 525–534.

Gangestad, S. W., Merriman, L. A., & Emery Thompson, M. (2010). Men's oxidative stress, fluctuating asymmetry and physical attractiveness. *Animal Behaviour*, *80*(6), 1005–1013.

Goto, T., Tamura, H., Kawai, T., Hoshino, T., Harada, N., & Kondo, T. (1986). Chemistry of Metalloanthocyaninsa. *Annals of the New York Academy of Sciences*, *471*(1), 155–173.

Gris, E., Ferreira, E., Falcão, L., & Bordignon-Luiz, M. (2007). Caffeic acid copigmentation of anthocyanins from Cabernet Sauvignon grape extracts in model systems. *Food Chemistry*, *100*(3), 1289–1296.

Huang, S. J., Sun, S. L., Feng, T. H., Sung, K. H., Lui, W. L., & Wang, L. F. (2009). Folate-mediated chondroitin sulfate-Pluronic® 127 nanogels as a drug carrier. *European Journal of Pharmaceutical Sciences*, *38*(1), 64–73.

Ichikawa, H., Ichiyanagi, T., Xu, B., Yoshii, Y., Nakajima, M., & Konishi, T. (2001). Antioxidant activity of anthocyanin extract from purple black rice. *Journal of Medicinal Food*, *4*(4), 211–218.

Jaruga, P., Zastawny, T. H., Skokowski, J., Dizdaroglu, M., & Olinski, R. (1994). Oxidative DNA base damage and antioxidant enzyme activities in human lung cancer. *FEBS Letters*, *341*(1), 59–64.

Jenner, P. (2003). Oxidative stress in Parkinson's disease. *Annals of Neurology*, *53*(S3), S26–S38.

Kähkönen, M. P., Hopia, A. I., Vuorela, H. J., Rauha, J. P., Pihlaja, K., Kujala, T. S., et al. (1999). Antioxidant activity of plant extracts containing phenolic compounds. *Journal of Agricultural and Food Chemistry*, *47*(10), 3954–3962.

Kim, H., & Na, K. (2010). Evaluation of succinylated pullulan for long-term protein delivery in poly (lactide-co-glycolide) microspheres. *Macromolecular Research*, *18*(8), 812–819.

Klaunig, J. E., Xu, Y., Isenberg, J. S., Bachowski, S., Kolaja, K. L., Jiang, J., et al. (1998). The role of oxidative stress in chemical carcinogenesis. *Environmental Health Perspectives*, *106*(Suppl. 1), 289.

Kong, J. M., Chia, L. S., Goh, N. K., Chia, T. F., & Brouillard, R. (2003). Analysis and biological activities of anthocyanins. *Phytochemistry*, *64*(5), 923–933.

Kowalczyk, E., Krzesiñski, P., Kura, M., Szmigiel, B., & Blaszczyk, J. (2003). Anthocyanins in medicine. *Polish Journal of Pharmacology*, *55*(5), 699–702.

Laleh, G., Frydoonfar, H., Heidary, R., Jameei, R., & Zare, S. (2006). The effect of light, temperature, pH and species on stability of anthocyanin pigments in four Berberis species. *Journal of Nutrition*, *5*, 90–92.

Lee, E. S., Park, K. H., Kang, D., Park, I. S., Min, H. Y., Lee, D. H., et al. (2007). Protein complexed with chondroitin sulfate in poly (lactide-co-glycolide) microspheres. *Biomaterials*, *28*(17), 2754–2762.

Mistry, T. V., Cai, Y., Lilley, T. H., & Haslam, E. (1991). Polyphenol interactions. Part 5. Anthocyanin co-pigmentation. *Journal of the Chemical Society, Perkin Transactions 2*, (8), 1287–1296.

Mohanraj, V., & Chen, Y. (2007). Nanoparticles – A review. *Tropical Journal of Pharmaceutical Research*, *5*(1), 561–573.

Montenecourt, B. S., & Eveleigh, D. E. (1979). Selective screening methods for the isolation of high yielding cellulase mutants of *Trichoderma reesei*. *Advances in Chemistry Series*, *181*, 289–301.

Newsholme, P., Haber, E., Hirabara, S., Rebelato, E., Procopio, J., Morgan, D., et al. (2007). Diabetes associated cell stress and dysfunction: Role of mitochondrial and non-mitochondrial ROS production and activity. *The Journal of Physiology*, *583*(1), 9–24.

Pietta, P. G. (2000). Flavonoids as antioxidants. *Journal of Natural Products*, *63*(7), 1035–1042.

Rice-Evans, C., Miller, N., & Paganga, G. (1997). Antioxidant properties of phenolic compounds. *Trends in Plant Science*, *2*(4), 152–159.

Rice-Evans, C. A., Miller, N. J., & Paganga, G. (1996). Structure–antioxidant activity relationships of flavonoids and phenolic acids. *Free Radical Biology and Medicine*, *20*(7), 933–956.

Seeram, N. P., Bourquin, L. D., & Nair, M. G. (2001). Degradation products of cyanidin glycosides from tart cherries and their bioactivities. *Journal of Agricultural and Food Chemistry*, *49*(10), 4924–4929.

Shi, Y., & Li, L. (2005). Current advances in sustained-release systems for parenteral drug delivery. *Expert Opinion on Drug Delivery*, *2*(6), 1039–1058.

Smith, M. A., Rottkamp, C. A., Nunomura, A., Raina, A. K., & Perry, G. (2000). Oxidative stress in Alzheimer's disease. *Biochimica et Biophysica Acta (BBA)*, *1502*(1), 139–144.

Wang, L. S., & Stoner, G. D. (2008). Anthocyanins and their role in cancer prevention. *Cancer Letters*, *269*(2), 281–290.

Zhang, L., Gu, F., Chan, J., Wang, A., Langer, R., & Farokhzad, O. (2007). Nanoparticles in medicine: Therapeutic applications and developments. *Clinical Pharmacology & Therapeutics*, *83*(5), 761–769.